

## Journal Pre-proofs

Original article

Removal of dithioerethiol (DTT) from water by membranes of cellulose acetate (AC) and AC doped ZnO and TiO<sub>2</sub> nanoparticles

Zahrah Alhalili, Chourouk Romdhani, Hajer Chemingui, Moêz Smiri

PII: S1319-6103(21)00087-9  
DOI: <https://doi.org/10.1016/j.jscs.2021.101282>  
Reference: JSCS 101282

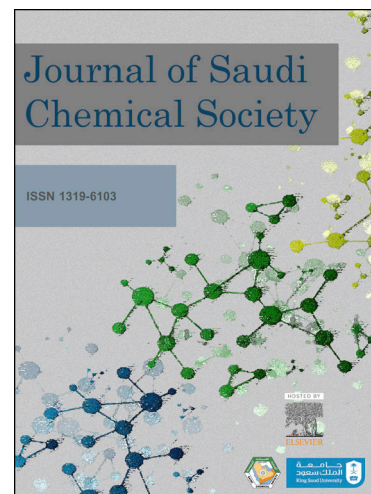
To appear in: *Journal of Saudi Chemical Society*

Received Date: 8 April 2021  
Revised Date: 10 May 2021  
Accepted Date: 10 June 2021

Please cite this article as: Z. Alhalili, C. Romdhani, H. Chemingui, M. Smiri, Removal of dithioerethiol (DTT) from water by membranes of cellulose acetate (AC) and AC doped ZnO and TiO<sub>2</sub> nanoparticles, *Journal of Saudi Chemical Society* (2021), doi: <https://doi.org/10.1016/j.jscs.2021.101282>

This is a PDF file of an article that has undergone enhancements after acceptance, such as the addition of a cover page and metadata, and formatting for readability, but it is not yet the definitive version of record. This version will undergo additional copyediting, typesetting and review before it is published in its final form, but we are providing this version to give early visibility of the article. Please note that, during the production process, errors may be discovered which could affect the content, and all legal disclaimers that apply to the journal pertain.

© 2021 Published by Elsevier B.V. on behalf of King Saud University.



**Removal of dithioterethiol (DTT) from water by membranes of cellulose acetate (AC) and AC doped ZnO and TiO<sub>2</sub> nanoparticles**

**Zahrah Alhalili<sup>1</sup>, Chourouk Romdhani<sup>2</sup>, Hajer Chemingui<sup>2</sup>, Moêz Smiri<sup>3\*</sup>**

*<sup>1</sup>Department of Chemistry, College of Sciences and Arts – Sajir, Shaqra University, Saudi Arabia*

*<sup>2</sup>Laboratory of Water, Membranes and Environment Biotechnology (LEMBE), Technopole of Borj Cedria (CERTE), Hammam-Lif 2050, Tunisia*

*<sup>3</sup>Department of Biology, College of Sciences and Arts – Sajir, Shaqra University, Saudi Arabia*

**\*Corresponding author: Moêz Smiri**

[almoez@su.edu.sa](mailto:almoez@su.edu.sa)

*College of Sciences and Arts – Sajir, Shaqra University, Saudi Arabia*

**Removal of dithioterethiol (DTT) from water by membranes**

**of cellulose acetate (AC) and AC doped ZnO and TiO<sub>2</sub>  
nanoparticles**

**ABSTRACT**

Dithioterethiol (DTT) is a typical example of substances that contain sulfur with adverse effects on human health. Membranes-based cellulose acetate is used for the separation processes of thiols after the addition of ZnO and TiO<sub>2</sub> nanoparticles. The measurement of permeability allows us to estimate the efficiency of membrane cleaning. The permeability increases from 8.82 L.h<sup>-1</sup>.m<sup>-2</sup>.bar<sup>-1</sup> for CA membrane to 20.77 L.h<sup>-1</sup>.m<sup>-2</sup>.bar<sup>-1</sup> for CA-TiO<sub>2</sub> and 21.96 L.h<sup>-1</sup>.m<sup>-2</sup>.bar<sup>-1</sup> for CA-ZnO membranes. For the permeability values of DTT, we noted that the CA-ZnO membrane has the highest permeability (50.66 L.h<sup>-1</sup>.m<sup>-2</sup>.bar<sup>-1</sup>). The CA-ZnO membrane changes from nanofiltration to ultrafiltration membrane. On the other hand, for the CA-TiO<sub>2</sub> modified membrane, the permeability decreases to 6.00 L.h<sup>-1</sup>.m<sup>-2</sup>.bar<sup>-1</sup>. The CA-TiO<sub>2</sub> membrane is in the category of reverse osmosis membranes. This variation is explained by the interaction between nanoparticles and DTT. The contact angles of the incorporated membranes decrease progressively with the addition of TiO<sub>2</sub> or ZnO-NPs. The low contact angle with water means high hydrophilicity, indicated that the addition of TiO<sub>2</sub> and ZnO improved the hydrophilicity of the membranes. The CA membrane had the highest contact angle with water of 92.64±1.5°. After the addition of 0.1 g of TiO<sub>2</sub> or ZnO, the contact angle of CA-TiO<sub>2</sub> and CA-ZnO was reduced to 86.7±0.2° and 70.51±1.5°, respectively. Both TiO<sub>2</sub> and ZnO caused strong hydrophilicity of membranes. From the elimination rates of DTT, it is concluded that there are optimal conditions of (1) Pressure P = 2 bars, (2) pH = 10 and (3) DTT concentration = 2 mM.

**KEYWORDS**

Cellulose acetate (CA)

The dioxide of titane ( $\text{TiO}_2$ )

Dithioerethiol (DTT)

Membrane

Sulfhydryl groups

Water

Zinc oxide ( $\text{ZnO}$ )

## 1. INTRODUCTION

Water pollution occurs due to various organic and inorganic materials such as pesticides, detergents, heavy metals, sulfhydryl groups (thiols -SH), and other toxic substances [1]. Sulfhydryl groups represent a real danger for the aquatic fauna and flora and caused serious problems for humanity [2]. Thiols present as functional groups of macromolecules such as proteins, but also free as small peptides, not bound to macromolecules, in the cytoplasmic space of cells and aquatic environments. These thiols are called non-protein thiols or low molecular weight thiols (LMWT). Dithiothreitol (DTT) is a typical example of substances that contain sulfur with adverse effects on human health (such as neurological effects and behavior modification and heart problems...), on the environment (including :disturbance of wildlife and alteration of water quality), and also on the wastewater treatment plant (such as corrosion and odor problems...).

A wide range of physical, chemical, and biological methods are used to remove sulfur [3]. Strategies for removing thiol from water include separation by membrane processes such as ultrafiltration and/or nanofiltration. In recent years, the membrane technologies used in separation processes have been improved by incorporating inorganic additives into the polymer material. Nanoparticles used to change polymer membranes are  $\text{SiO}_2$ ,  $\text{Al}_2\text{O}_3$ ,  $\text{Fe}_3\text{O}_4$ ,  $\text{ZrO}_2$ ,  $\text{ZnO}$ , and  $\text{TiO}_2$ . These nanoparticles can be a challenge to solve water pollution problems.

According to Koval (2005) [4], he defined thiols as a set of organosulfur molecules having a sulfhydryl group (-SH) bonded to a carbon atom. This -SH group acts at the level of different cellular pathways, both in unicellular organisms and in organisms of more complex organizational levels [5]. Thiols

can be present as functional groups for macromolecules such as proteins, but also free as small peptides, not bound to macromolecules, in the cytoplasmic space of cells and aquatic environments. These thiols are then called non-protein thiols or low molecular weight thiols (LMWT). This distinctive class of LMWT will be discussed. It plays a key role in the biogeochemical cycling of sulfur, allowing a transition from inorganic to organic forms of sulfur [6]. Many thiols have strong garlic-like odors. The odors of thiols, especially those of LMWT, are often strong and repulsive. Skunk spraying consists mainly of thiols and low molecular weight derivatives [7]. These compounds are detectable by the human nose at concentrations of only 10 parts per billion [8]. Thiols show a weak association with hydrogen bonding, both with water molecules and with each other. Therefore, they have lower boiling points and are less soluble in water and other polar solvents than alcohols of similar molecular weight. For this reason, thiols and isomers of the thioether functional groups have similar solubility characteristics and boiling points, which is not the case for alcohols and their ether isomers. Thiols are molecules close to alcohols, but where the oxygen atom is replaced by a sulfur atom. They are therefore characterized by one or more sulfhydryl groups -SH. Oxygen and sulfur have similar chemical properties because they belong to the same group in the periodic table. Thiols form thioethers, thioacetals, and thioesters, in which one or more oxygen atoms are replaced by a sulfur atom [9]. Many thiols are colorless liquids with a pKa between 8 and 11 [10]. It is important to note that within certain proteins, the environment may further promote the deprotonation of thiols, which will therefore appear rather in the form of thiolate -S- groups [11]. Thiols can easily be oxidized either to deprotonated sulfenic acids -SO- or in pairs to form

disulfide bridges RSSR' [11]. There are several forms of a thiol such as methanethiol, coenzyme, lipoamide, cysteine, and dithiothreitol (DTT). DTT is a small redox molecule, also known as Cleland's reagent. Its gross chemical formula is  $C_4H_{10}O_2S_2$  [12]. The molecular structure of the reduced form of this compound is R-S-H. DTT is a reducing agent mainly used to protect free SH groups from oxidation during protein isolation or other biochemical procedures. Due to its low redox potential (-0.33 V at pH 7), the pKa of thiol groups is 9.2. DTT maintained free SH groups in a reduced state and quantitatively reducing disulfide bridges [13].

Sulfur is the chemical element with atomic number 16, symbol S. It is a member of the chalcogen group. It is a multivalent non-metal that is abundant, tasteless, and insoluble in water. Sulfur is mostly known as yellow crystals and is found in many minerals (sulfide and sulfate) and even in the native form [14,15]. Sulfides are also present in industrial wastes from refineries, petrochemical plants, gas plants, paper mills, heavy water plants, and tanneries [16]. During various processes, sulfur compounds are released into the environment which can have harmful consequences for animals and humans [17].

Membrane techniques operating in liquid media and using pressure as a driving force are as follows (1) Microfiltration (MF) defined as a solid/liquid separation process. For this reason, this technique is used for the removal of macro solutes present in effluents or water for domestic, industrial (electronics), or medical use [18]. (2) Ultrafiltration is the intermediary between MF and NF, it has a selectivity of both physical origin by the transfer coefficient and chemical origin by the partition coefficient [19]. The main industrial

applications of ultrafiltration are as the following [20] (i) The treatment of paint baths by electrophoresis, (ii) Treatment of degreasing baths (removal of suspended solids (SS) and emulsified oil), (iii) Recovery of metal cations by complexation-assisted ultrafiltration, (vi) Protein standardization of milk, (v) The concentration of whey proteins and (vi) Membrane bioreactors. (3) Nanofiltration lies between reverse osmosis and ultrafiltration. It allows the separation of components with a solution size close to that of the nanometre (i.e. 10 Å), hence its name. Monovalent ionized salts and non-ionized organic compounds with a molar mass of less than about 200 - 250 g/mol are not retained by this type of membrane. Multivalent ionized salts (calcium, magnesium, aluminum, sulfates...) and un-ionized organic compounds with a molar mass greater than about 250 g/mol are, on the other hand, strongly retained [21]. (4) Reverse osmosis uses dense membranes that allow water to pass through and stop all salts [22]. Osmosis is a phenomenon that tends to balance the concentration of solutes on either side of a semi-permeable membrane. To reverse the passage of the solvent and increase the concentration difference, a pressure higher than the osmotic pressure must be applied [23]. A membrane is defined as a thin semi-permeable layer that acts as a selective barrier that separates dissolved or undissolved substances under the action of chemical (concentration ...) or physical (pressure) force. In general, constituents that are smaller than the pores of the membrane can pass through the membrane under the effect of applied pressure, while larger substances and molecules are retained by the membrane [24]. The vast majority of ultrafiltration and microfiltration membranes consist of organic membranes [25-28]. The structure of the membrane is an important factor because it will govern the mechanism of

transport of the solutes and thus influence the field of application of this membrane. The diffusion of the solutes will therefore depend on their diffusivity and solubility across the membrane [29]. The separation of molecules in solution is therefore done according to their size and pore size distribution if the membrane is asymmetric [30]. Membrane geometry is often equated with module geometry. Thus, it is common to speak of a flat, tubular, or hollow fiber membrane. The multi-channel module (monolith) made of assembling parallel tubes in the same matrix represents the current optimized shape [31]. Hollow fiber membranes are membranes with a diameter of less than 0.1  $\mu\text{m}$  and therefore the risk of obstruction is very high. These membranes can only be used for the treatment of water with little suspended solids. The packing density is very high [30,31].

Most of the studies have focused on  $\text{TiO}_2$  nanoparticles.  $\text{ZnO}$  nanoparticles also have many remarkable properties such as (1) easily absorb hydrophilic hydroxyl groups (-OH) to become hydrophilic [32], (2) have a high specific surface compared to nano- $\text{TiO}_2$  due to its crystallographic structure [33], (3) have excellent antibacterial and antifungal characteristics, thanks to their valuable ultraviolet resistance and photocatalytic properties [34], (4)  $\text{ZnO}$  nanoparticles have a low cost and are less toxic than  $\text{TiO}_2$  nanoparticles, (5)  $\text{ZnO}$  nanoparticles are easily processed compared to  $\text{TiO}_2$  nanoparticles, (6)  $\text{TiO}_2$  and  $\text{ZnO}$  nanoparticles are well known for their potential cytotoxicity to living organisms [35], (7)  $\text{TiO}_2$  is stable, non-toxic and inexpensive, and (8) nanoparticles of  $\text{TiO}_2$  [18], and  $\text{ZnO}$  [36,37] have antibacterial properties.  $\text{TiO}_2$  is widely used in the fields of environment and energy, air treatment and water purification systems, sterilization, hydrogen release, and photo-electrochemical

conversion [38]. ZnO nanoparticles are used in the production of antibacterials, cosmetics, electronics, paint pigments, pharmaceuticals [39], photocatalytic degradation of dyestuffs in water [40] rubber additives, and transparent sun filters [41], as well as their potential use as photodetectors [42]. The membrane pore size varies from a few microns in microfiltration to one nanometer in nanofiltration. The porosity of a membrane is never perfectly uniform. The solvent transfer mechanism is more solution/diffusion than convection: water is not only pushed to infiltrate through the membrane, but also it diffuses through the membrane material. The polymer structure of the material changes depending on the activation energies and therefore on the temperature. The selectivity of these membranes depends on the chemical affinity of the material with the different compounds that pass through the membrane [43]. The membrane cut-off corresponds to the molar mass of the smallest compound with observed retention of 90%. It is expressed in Da or kDa ( $1 \text{ Da} = 1 \text{ g} \cdot \text{mol}^{-1}$ ). It is a quantity whose simple definition hides the difficulty of unambiguous determination. Indeed, the retention of a solute does not only depend on its size, but also hydrodynamics and the physicochemical environment play an important role if charged solutes are in the feed solution [44]. The presence of sulfur in wastewater causes serious odor and corrosion problems in sewage systems. This work proposed to study the elaboration of cellulose acetate polymer-based membranes for their application in the removal of a synthetic thiol. Membranes of cellulose acetate are used for the separation processes of DTT after the addition of ZnO and TiO<sub>2</sub> nanoparticles.

## 2. MATERIALS AND METHODS

## 2.1. Materials

Cellulose acetate (CA) extra pure with acetyl content ranging from 29 to 45% from lobachemie, dimethylformamide pure (DMF), and PEG 1000(purity 99%) was obtained from Merck which were used as received to prepare the casting solution. Zinc Acetate dehydrate ( $\text{Zn}(\text{OAc})_2 \cdot 2\text{H}_2\text{O}$ ), and sodium hydroxide (NaOH) were obtained from Sigma Aldrich. The  $\text{TiO}_2$  nanopowder was purchased from US Nano with a particle size of 80 nm.

## 2.2. Nanoparticle preparation

In optimal conditions, ZnO NPs were synthesized according to other reported works through low-temperature co-precipitation. 25 mL of NaOH solution (2M) was added dropwise for 30 minutes to 25 mL of  $\text{Zn}(\text{OAc})_2 \cdot 2\text{H}_2\text{O}$  solution 0.2 M, and the mixture was vigorously stirred for 2 h at 60 °C. The resulting precipitate was centrifuged to separate ZnO powder from solvent, washed several times with distilled water and ethanol, finally dried at 80 °C for 5 h, and then treated at a calcination temperature of 400 °C for 1 h.

## 2.3. Membrane preparation

CA/Nanoparticles mixtures membranes were prepared with the various compositions indicated in Table 1 using the phase inversion method. For the membranes with 0/4, and 0.1/4 NPs/ CA ratios (w/w), 0 g, 0.1 g of nanoparticles were added to DMF (dimethylformamide) solution (20 g) under quick stirring. For 3 hours, the mixture solution was ultrasonicated and stirred. Subsequently, 4 g of CA was added to each mixture while stirring and mixed thoroughly for 72 hours at 70 °C. To get the casting suspension, approximately 1 g of the pore-forming reagent (PEG- 1000) was added to each combination solution and

stirred for 12 hours at 70 °C. The casting suspension was static to eliminate the air bubbles before use for 24 hours at 70 °C. The prepared casting solution was poured onto a clean glass plate and dispersed using Filmographe Doctor Blade 360099003 (Brave Instrument, Germany) at a thickness set at 0.25 mm. The nascent membrane was evaporated in the air for 15 seconds at room temperature before being immersed in a deionized-water precipitation bath. After complete precipitation, all prepared membranes were transferred to a drip-washing water bath for 3 days at room temperature to remove any remaining solvents from the membrane structures. The prepared membranes were then put to the test.

#### 2.4. Characterizations

A Philips x-pert X-ray diffractometer, equipped with a radiation source Cu ( $\lambda_{Cu} = 0.154$  nm), has been used to investigate the crystal structure of the prepared powder (ZnO NPs). At a scanning rate of  $0.02^\circ$ , the  $2\theta$  range was varied between  $20^\circ$  and  $70^\circ$ . The crystallite size  $D$  was calculated from the line broadening using Scherrer's relation:

$D = \frac{0.9 * \lambda}{\beta \cos\theta}$ , where  $\lambda$  is the X-ray wavelength,  $\beta$  is the angular width of the peak at

half its maximum intensity (full-width at half-maximum (FWHM)) corrected for instrumental broadening and is the Bragg angle of the corresponding peak. The morphology and size distribution were characterized by scanning electron microscopy (SEM)(Philips XL30 SFEG) and transmission electron microscopy (TEM) measurement in the TECHNAI-20- Philips instrument. The Infrared spectrum has been registered by a Perkin-Elmer (FTIR 2000) spectrometer using KBr pellets in the region of  $4000-400$   $\text{cm}^{-1}$ . The Attention Theta optical tension-meter determines the membrane hydrophobicity character via the

measurement of the membrane contact angle (CA). The measurements were performed using ultrapure water drop (5  $\mu\text{L}$ ). For all membranes, at least 3 measurements were taken and the average value and the corresponding standard deviation were then calculated.

## 2.5. Water content and porosity

The equilibrium water content (EWC) of samples was determined by immersing them in water for 24 hours and weighing them (WW) [45]. After drying overnight at 75  $^{\circ}\text{C}$ , the samples were weighed again ( $w_d$ ). After that, the EWC was determined using the following equation [46]:

$$EWC = \frac{ww - wd}{ww} * 100 \quad (2)$$

Membranes porosity ( $\% \varepsilon$ ), defined as the ratio between the volume of voids present in the membrane and the overall membrane volume, was measured by the gravimetric method as reported in the literature [47], which consisted of weighing the membrane in dry and wet (kerosene for 24 h) conditions. The porosity was determined using the following equation (3):

$$\% \varepsilon = \frac{(ww - wd)/\rho_i}{\frac{(ww - wd)}{\rho_i} + wd/\rho_c} * 100 \quad (3)$$

Where  $w_w$  and  $w_d$  are the weight of the wet and dry membrane, respectively.  $\rho_i$  is the kerosene density (0.82  $\text{g}\cdot\text{cm}^{-3}$ ) and  $\rho_c$  is the CA density (1.28  $\text{g}\cdot\text{cm}^{-3}$ ). Three measurements were taken for each membrane, and the average values and standard deviations were calculated.

## 2.6. Frontal filtration pilot

The performance of the prepared membranes was analyzed through a cross-flow system. Figure 1 represents the scheme of the experimental system, consisted of a filtration cell, a storage tank, and a magnetic stirrer.

## 2.7. Experimental protocol

A volume of 200 mL of the solution to be treated was introduced into the feed tank. The pressure applied to the solution varied from 2 to 5 bar through a nitrogen flow. The filtration model was frontal type and the recirculation speed is 1 m/s. The volume of permeate samples collected (not recycled) does not exceed 30 mL for each test, and the solution was replenished at each pressure value. After each test, the membrane held in the module was washed by the circulation of ultrapure water to the reference state. As for the UF membrane, it must be conditioned, at the time of first use, by immersion in pure water for 24 hours. It was then subjected to a pure water filtration pressure equivalent to the maximum pressure of use to avoid any modification such as possible compaction that could be caused by the high pressures.

The selectivity of a membrane for a given substance depends on its nature and structure, the chemical environment near the membrane, and the chemical properties of the substance to be separated.

The selectivity is expressed by a retention rate TR defined by:

$$TR = 1 - C_p/C_a$$

There are two extreme values of the TR (values expressed as percentages):

**TR =0%** means that the solute is not retained by the membrane at all;

**TR=100%** means that the solute is fully retained by the membrane.  $C_p$  and  $C_a$  are successively the concentrations of a solute in the permeate and the feed [48].

The permeability ( $L_p$ ) of a membrane is an intrinsic characteristic of the membrane that depends on its structure. In practical terms, permeability can be defined as the ratio between the permeate flow ( $J_p$ ) and the effective transmembrane pressure difference ( $\Delta P_m$ ) [49].

$$L_p = J_p / \Delta P_m$$

$L_p$ : permeability

$J_p$ : the permeate flow

$\Delta P_m$ : the effective transmembrane pressure

In the case of membrane techniques, the flow of the fluid to be filtered can be continuous and tangential. The flow fraction of the fluid flowing through the membrane is called the conversion rate of the separation operation [22].

$$Y = Q_p / Q_a$$

$Y$  : conversion rate

$Q_p$ : permeate flow rate

$Q_a$ : feed rate

The permeate flux was evaluated by the equation:

$$J = V / S * t$$

$J$ : permeate flux ( $L/m^2h$ )

$V$ : volume of accumulated permeate (L)

$S$ : Membrane surface area ( $m^2$ )

t: filtration time (h)

## 2.8. Determination of DTT concentration

DTT was determined in the sample at 412 nm using 5,5-dithiol-bis-(2-nitrobenzoic acid) (DTNB) [50]. We used DTT as a standard.

## 3. RESULTS AND DISCUSSION

This work is devoted to the study of the removal of synthetic thiols through three types of membranes. The filtration tests in the frontal mode were realized using water from three treatment plants.

### 3.1. Analysis of zinc oxide nanoparticle

Figure 2a depicts the XRD patterns of ZnO nanoparticles synthesized via the co-precipitation method. The XRD pattern revealed the orientation and crystalline nature of zinc oxide nanoparticles. The peak position with  $2\theta$  values of  $31.7^\circ$ ,  $34.4^\circ$ ,  $36.2^\circ$ ,  $47.5^\circ$ ,  $56.6^\circ$ ,  $62.8^\circ$ ,  $65.5^\circ$ ,  $67.9^\circ$ ,  $68.8^\circ$ ,  $72.3^\circ$ , and  $76.7^\circ$  are indexed as (100), (002), (101), (102), (110), (103), (200), (112), (201) and (202) planes. In comparison to the data from JCPDS card No. 36-1451; all of the observed peaks were coordinated with the hexagonal phase (Wurtzite structure). There were no other peaks associated with impurities observed, confirming that the synthesized powder is pure ZnO. Similar XRD results have been reported in the literature for ZnO nanoparticles [51, 52]. The average crystalline size of ZnO was estimated to be 35 nm based on the line width broadening of the XRD peak using the Debye-Scherrer method [53]. Figure 2b shows that the particles in general spherical shape had no agglomeration and were similar in a spherical shape to the results obtained in previous research [54]. Simultaneously, the TEM

image of ZnO nanoparticles prepared under optimal conditions was shown in Figure 2c. The average particle size of ZnO nanoparticles was approximately 35 nm, which was consistent with XRD data. The results obtained from this study seemed to be compatible with those obtained by Chemingui et al [54]. Figure 2d shows the FTIR spectrum of nanoparticles from ZnO registered in the area of 4000-400  $\text{cm}^{-1}$ . In the synthesized ZnO NPs there were two large bands of absorption: the band at 3450  $\text{cm}^{-1}$  correlates to the presence of hydroxyl groups – OH, and the band between 400 and 600  $\text{cm}^{-1}$  contributes to the bending vibration of ZnO [52,55].

### 3.2. Characterization of membrane

Figure 3 summarized the effect of NPs on the water content (%) and porosity (%) of CA membranes. The porosities of NPs/CA hybrid membranes are higher than that of the CA membrane. The porosity increases with the contribution of nanoparticles in the membrane. It is known that high porosity is favorable to water flux. It is widely accepted as a general rule that increased exchange rates between water and solvent can result in more porous membranes and vice versa [56]. The reasons for the porosity variable are discussed further below. The presence of nano-ZnO causes two effects: hydrophilicity and viscosity. During the phase inversion process, hydrophilic nano-ZnO easily draws water into the casting suspension.

To investigate the efficacy of various contents of ZnO NPs on the CA ultrafiltration membrane, Scanning Electron Microscopy (SEM) analysis was utilized. CA membranes morphology was examined by (SEM), the obtained images of cross-section and top surface were reported in Figure 4. As seen in Figure 4a, CA NF membranes showed an asymmetrical morphology consisting

of a dense layer supported on a porous sub-structure characterized by the presence of macro voids, whereas both the surfaces appeared uniform, smooth and dense. It is identified that the up-layers of the membranes restrict the flux and determine the rejection [57]. As seen from Figure 4b, by adding ZnO NPs, the number of pores in the matrix membranes increases. Also, in the sub-layer, the macro-void volume of all the modified membranes seems to be larger than the unfilled CA. The reason for this phenomenon can be a higher chance of agglomeration for ZnO NPs. Furthermore, as ZnO NPs amount rises, polymeric solution viscosity increases. Although the viscosities were not measured precisely, an increase in viscosity of the polymeric solution with the addition of the nanoparticles was visually detected and has been reported in the same papers [58].

The FTIR analysis results were used to investigate the interaction between ZnO and cellulose acetate. The FTIR spectra of M0 and composite CA/ZnO membrane are shown respectively in Figures 5a and b. The main characteristic bands of CA have been given as follows: The appearance of hydroxyl groups can be likened to the characteristic absorption peak at  $3500\text{ cm}^{-1}$  and the peaks at  $1743$ ,  $1270$  and  $1050\text{ cm}^{-1}$  correlate to the stretching of C–O group, aromatic ring group and C–O bond of the  $-\text{CH}_2-\text{OH}$  group, respectively [59]. In Figure 5b, in addition to the CA characteristics peak, a new peak around  $477\text{ cm}^{-1}$  is assigned to the Zn–O vibration, proving the existence of ZnO in the membrane. When the IR spectra of the ZnO/CA composite membrane were compared to those of pure CA membrane, the characteristics peak of the  $-\text{OH}$  group was shifted to  $3451\text{ cm}^{-1}$  from  $3450\text{ cm}^{-1}$ , as seen in the figure. Peaks located at  $1744$ ,  $1271$ , and  $1051\text{ cm}^{-1}$  each show a similar change. The identified peak shifts may be explained by

the formation of complexes between ZnO and CA [60].

### 3.4. Optimization of DTT removal conditions by ultrafiltration

The purpose of this section was to determine the optimal conditions (pressure, concentration, pH, and time) for the removal of DTT.

#### 3.4.1. Water permeability

The permeate flow was measured during the filtration of pure water, at different transmembrane pressures between 0 and 5 bars, across different membranes (Table 2). The results in Figure 6A show that the permeate flow is proportional to the applied pressure.

The permeability values obtained, at 25 °C, are as follows:

$$L_p(\text{CA}) = 8.82 \text{ L.h}^{-1}.\text{m}^{-2}.\text{bar}^{-1}$$

$$L_p(\text{CA-TiO}_2) = 20.77 \text{ L.h}^{-1}.\text{m}^{-2}.\text{bar}^{-1}$$

$$L_p(\text{CA-ZnO}) = 21.96 \text{ L.h}^{-1}.\text{m}^{-2}.\text{bar}^{-1}$$

The measurement of permeability also allows estimating the efficiency of membrane cleaning. From the permeability values, it can be noted that membranes based on ZnO and TiO<sub>2</sub> have a higher permeability (Figure 6A). The permeability increases from 8.82 L.h<sup>-1</sup>.m<sup>-2</sup>.bar<sup>-1</sup> for (CA membrane) to 20.77 L.h<sup>-1</sup>.m<sup>-2</sup>.bar<sup>-1</sup> for (TiO<sub>2</sub> membrane) and 21.96 L.h<sup>-1</sup>.m<sup>-2</sup>.bar<sup>-1</sup> for ZnO membrane. The result shows that membrane modifications by nanoparticles lead to an increase in pore size. It is therefore a pyrogenic additive, i.e. it increases the pores of the membranes, which increases the permeability. The CA-ZnO and CA-TiO<sub>2</sub> membranes change from nanofiltration to ultrafiltration membranes. Zinc oxide-modified membranes have a positive

effect. The influence of TiO<sub>2</sub> and ZnO nanoparticles on the permeation properties of PSf membranes has been studied at 32% of PSf and 0.125% of nanoparticles [61]. Results confirm our findings that the addition of nanoparticles has a positive influence on the permeation properties of membranes. Membranes mixed with ZnO nanoparticles have a better improvement of water flow compared to treated membranes and membranes mixed with TiO<sub>2</sub> nanoparticles [62].

#### 3.4.2. Membrane permeability for DTT

The permeate flow was measured during the filtration of DTT solution, at different transmembrane pressures between 0 and 5 bars using CA, CA-ZnO, and CA-TiO<sub>2</sub> membranes. Results in Figure 6B show that the permeate flow is proportional to the applied pressure. Permeability values obtained at 25 °C are as follows:

$$L_p(\text{CA}) = 9,33 \text{ L.h}^{-1}.\text{m}^{-2}.\text{bar}^{-1}$$

$$L_p(\text{CA-TiO}_2) = 6,00 \text{ L.h}^{-1}.\text{m}^{-2}.\text{bar}^{-1}$$

$$L_p(\text{CA-ZnO}) = 50,66 \text{ L.h}^{-1}.\text{m}^{-2}.\text{bar}^{-1}$$

From the permeability values for DTT, we noted that the CA-ZnO membrane has the highest permeability. The permeability increases from 9.33 to 50.66 L.h<sup>-1</sup>.m<sup>-2</sup>.bar<sup>-1</sup> between CA membrane and CA-ZnO membrane. The CA-ZnO membrane changes from nanofiltration to ultrafiltration membrane. On the other hand, for the CA-TiO<sub>2</sub> modified membrane, the permeability decreases from 9.33 to 6.00 L.h<sup>-1</sup>.m<sup>-2</sup>.bar<sup>-1</sup>. The CA-TiO<sub>2</sub> membrane is in the category of reverse osmosis membranes. This variation is explained by the interaction

between nanoparticles and DTT.

### 3.4.3. Contact angle

As shown in [Figure 7](#), the contact angles of the incorporated membranes decrease progressively with the addition of TiO<sub>2</sub> or ZnO-NPs. The low contact angle with water means high hydrophilicity, indicated that the addition of TiO<sub>2</sub> and ZnO can improve the hydrophilicity of the membranes. However, the change in hydrophilicity may be related to the type of NPs. The CA membrane had the highest contact angle with water of 92.64±1.5°. After the addition of 0.1 g of TiO<sub>2</sub> or ZnO, the contact angle of CA-TiO<sub>2</sub> and CA-ZnO was reduced to 86.7±0.2° and 70.51±1.5°, respectively. Both TiO<sub>2</sub> and ZnO caused strong hydrophilicity of membranes.

**3.5. Study of thiol retention by ultrafiltration membrane assisted by ZnO and TiO<sub>2</sub> nanoparticles** The retention efficiency of thiols by nanoparticle-assisted ultrafiltration was determined using two parameters: the permeate flux  $J_p$  (L.h<sup>-1</sup>.m<sup>-2</sup>) and the retention rate R (%).

**3.5.1. Pressure effect on thiol retention by ultrafiltration membrane assisted ZnO and TiO<sub>2</sub> NPs** The variation of DTT retention rate as a function of transmembrane pressure was studied at different pressures from 2 to 5 bars. The concentration of thiol is fixed at 3 mM. According to [Figure 8A](#), retention is higher at 2 bar and then decreases as the pressure increases. During filtration, the retained species gradually accumulate on the surface of the membrane under the effect of pressure. This observation indicates that the retention of DTT is essentially linked to the complexation of thiol molecules by

CA. Choi et al. (2020) [63] suggested that thiol was incorporated onto the surface of cellulose nanofibers by chemisorption of each doubly charged metal ion that occurs with two thiol groups. Above a certain pressure, the driving forces of the solute become greater than the surface forces, as a result, the transport of solute increases, resulting in a decrease in the retention rate. We recorded good retention of 99.98% at 2 bar pressure for the CA and CA-ZnO-based membranes and less for the TiO<sub>2</sub> based membrane. This could be due to the difference in solubility of the two nanoparticles and as indicated in the chemical safety data sheet that titanium dioxide is poorly soluble in water and in solutions that contain concentrated sulfur (H<sub>2</sub>SO<sub>4</sub>) [64] while Zinc oxide has a high solubility in water [65].

### **3.5.2. pH effect on thiol retention by ultrafiltration membrane assisted ZnO**

**and TiO<sub>2</sub> NPs** We have considered an initial concentration for a pH range of 2-10 while maintaining a constant temperature of 25 °C. The pH of the solution is set by adding HCl (0.1 M) or NaOH (0.1 M), under stirring. According to Figure 8B, it can be seen that at a basic pH, there is a very high removal of DTT. At pH 10, retention is about 99.5% for CA, 88.5% for CA-ZnO, and 97.90% for CA-TiO<sub>2</sub> membranes. The retention rate of cellulose acetate-based membrane is higher than that of membrane mixed ZnO at pH 10. The variation in thiol retention as a function of pH can be explained by the interaction between thiol and cellulose acetate. Thiol (sulfhydryl group) is essentially in the ionic form SO<sub>4</sub><sup>2-</sup> while ZnO and TiO<sub>2</sub> are positively charged and are mainly in the neutral form at low pH equal to 2 and 4 which explains the low retention rates. The increase in pH leads to an increase in the cationic groups which favor the formation of the thiol-cellulose acetate

complex by electrostatic interaction between  $\text{Zn}^{2+}$ ,  $\text{Ti}^{4+}$ , and  $\text{SO}_4^{2-}$ . Studies on the effect of zinc oxide and titanium dioxide nanoparticles on supported lipid bilayers demonstrated the variation of the zeta potential of ZnO with a pH of 7-8.5, the dispersions are stable and positively charged (pH 7.4 ~ +3 mV) [66]. It is known that low zeta potentials tend to coagulate or flocculate the ZnO suspension. In variations of the zeta potential of  $\text{TiO}_2$  with a pH of 5 to 9, the dispersions are stable and the surface is positive (with a pH of 7.4 ~ 33 mV). In this case, a high zeta potential will confer stability to  $\text{TiO}_2$ , i.e. the suspension resists aggregation [67].

### ***3.5.3. Effect of DTT concentration on thiol retention by ultrafiltration***

***membrane-assisted ZnO and  $\text{TiO}_2$  NPs*** Results in Figure 8C show that thiol retention rates decrease with increasing DTT concentrations. It appears that the presence of high thiol concentration reduces the electrostatic interaction between thiol and cellulose acetate. On the other hand, Zn and Ti ions compete with DTT in the complexation process. Despite the addition of large amounts of DTT, retention rates remain high in the order of 99.67% at 2 mM. It can be seen that the removal of sulfur is perfect at a concentration of 2 mM and that the CA-ZnO and CA- $\text{TiO}_2$  membranes give the best removal results. In the absence of a precise study, we can make the hypothesis that the force of the charges has become important in ZnO and  $\text{TiO}_2$  based membranes. Previous results confirmed that the nanoparticle-membrane interaction depends on the nanoparticle charge as well as the zeta potential. While, cationic nanoparticles are known to penetrate through the membrane [68].

### ***3.5.4. Effect of time on thiol retention by ultrafiltration membrane assisted***

***ZnO and TiO<sub>2</sub> NPs under different pressures, DTT concentrations, and pH.***

According to [Figure 9](#), DTT treatment time decreases with increasing pressure and increases with increasing pH and concentration. The ZnO-modified membrane takes less time at few seconds than other membranes to process the synthetic solution because the pore size of the CA-ZnO membrane is larger than the CA-TiO<sub>2</sub> membrane. **The CA membrane exhibited effective and rapid adsorption behavior toward heavy metal ions in aqueous solutions as a function of the thiol concentrations, pressure, and pH [63].**

***3.5.5. Identification of thiols retention by ultrafiltration membrane assisted******ZnO and TiO<sub>2</sub> NPs using the fluorescence spectrum***

The fluorescence intensity gives a general idea about the characteristics of thiols and concerning the efficiency of the membranes that give the best sulfur removal. It can be seen from [Figure 10](#) that the intensity of fluorescence as a function of pressure, concentration, and pH gradually decreases for all three parameters, and the ZnO- modified membrane eliminates better than the other membranes. The retention rate depends on the physicochemical parameters. From the elimination rates, it is concluded that there are optimal conditions to have a better synthetic result, these conditions are the following: (1) Pressure P = 2 bars, (2) pH = 10, and (3) DTT concentration = 2 mM.

**4. CONCLUSION**

This work proposed to study the elaboration of cellulose acetate polymer-based membranes for their application in the removal of a synthetic thiol. The results obtained show that the ZnO-modified membrane gives a good synthetic sulfur

removal efficiency at optimal conditions of pressure at 2 bars, pH 10, and thiol concentration of 2 mM. We found that a synthetic sulfur removal membrane treatment gives better retention of 99.67 % at 2 mM. The characteristics of the cellulose acetate membrane under the influence of ZnO or TiO<sub>2</sub> nanoparticles were tested by fluorescence correlation spectroscopy. It was found the significant reduction of the mobility of sulfur diffusion, which can be explained by the binding of ZnO-sulfur aggregates, as a function of the ZnO concentration. TiO<sub>2</sub> has little effect on the mobility of sulfur diffusion. The addition of nanoparticles to membranes improves the water purification capacity by promoting a good separation of sulfur, more particularly by ZnO NPs.

## REFERENCE

- [1] T. Missaoui, M. Smiri, A. Hafiane Reserve Mobilization, Membrane Damage and Solutes Leakage in Fenugreek Imbibed with Urban Treated Wastewater. *Bulletin of Environmental Contamination and Toxicology*. 103 (2019) 461–467.
- [2] O.P. Ajsuvakova, A.A. Tinkov, M. Aschner, J.B.T. Rocha, B. Michalke, M.G. Skalnaya, G. Björklund, Sulfhydryl groups as targets of mercury toxicity. *Coordination Chemistry Reviews*. 417 (2020) 213343. doi:10.1016/j.ccr.2020.213343
- [3] A. Hidalgo-Vivas, B. H. Cooper, Sulfur removal methods. *Handbook of Fuel Cells*. (2010). doi:10.1002/9780470974001.f302016
- [4] I.V. Koval, Synthesis, Structure, and Physicochemical Characteristics of Thiols. *Russian Journal of Organic Chemistry*. 41 (2005) 647-664. <https://doi.org/10.1007/s11178-005-0220-0>
- [5] M. Smiri, S. Boussami, T. Missaoui and A. Hafiane, The Cadmium-Binding Thioredoxin O Acts as an Upstream Regulator of the Redox Plant Homeostasis.

- Redox State as a Central Regulator of Plant-Cell Stress Responses. Springer International Publishing Switzerland. (2016) 275–296. [https://doi.org/10.1007/978-3-319-44081-1\\_13](https://doi.org/10.1007/978-3-319-44081-1_13).
- [6] M.O. Andreae and W.A. Jaeschke, Exchange of Sulphur between Biosphere and Atmosphere over Temperate and Tropical Regions. Sulphur cycling on the continents: Wetlands, terrestrial ecosystems, and associated water bodies (1992).
- [7] W.F. Wood, B.G. Sollers, G.A. Dragoo and J.W. Dragoo, Volatile Components in Defensive Spray of the Hooded Skunk, *Mephitis macroura*. Journal of Chemical Ecology 28 (9) (2002) 186570. [doi: 10.1023/a:1020573404341](https://doi.org/10.1023/a:1020573404341).
- [8] W.F. Wood and K.P. Joest, Major volatile compounds from the anal gland of the long-tailed weasel. Biochemical Systematics and Ecology 36 (2008) 588-589. [DOI: 10.1016/j.bse.2008.01.005](https://doi.org/10.1016/j.bse.2008.01.005).
- [9] M. Smiri and J. El Ghoul, Role for Plant Thioredoxin in Cd<sup>2+</sup> Chelation. International Journal of Vegetable Science 18(1), 93-105. (2012). [DOI: 10.1080/19315260.2011.579692](https://doi.org/10.1080/19315260.2011.579692).
- [10] M. Smiri, N. Jelali and J. El Ghoul, Role for plant peroxiredoxin in cadmium chelation. Journal of Plant Interactions 8(2) (2013) 125-133 [DOI: 10.1080/17429145.2012.689865](https://doi.org/10.1080/17429145.2012.689865).
- [11] M. Smiri, N. Jelali and J. El Ghoul, Cadmium affects the NADP-thioredoxin reductase/thioredoxin system in germinating pea seeds. Journal of Plant Interactions 8(3) (2013) 255-262. [DOI: 10.1080/17429145.2012.711489](https://doi.org/10.1080/17429145.2012.711489).
- [12] M. Smiri, A. Chaoui and E.E. Ferjani, Interaction Between Heavy Metals and Thiol-linked Redox Reactions in Germination. Pakistan Journal of Biological Sciences 13 (2010) 877-883. [DOI: 10.3923/pjbs.2010.877.883](https://doi.org/10.3923/pjbs.2010.877.883).
- [13] B. Cardey, S. Foley, and M. Enescu, Theoretical study of the mechanisms of thiol oxidation in a medium of biological interest. Journal of Physical Chemistry A 111(50) (2008) 13046-52. [DOI: 10.1021/jp0731102](https://doi.org/10.1021/jp0731102).
- [14] P. Pignatti, M. Delmastro and L. Perfetti, Cadmium Affects the Glutathione/Glutaredoxin System in Germinating Pea Seeds. Journal

- of Allergy and Clinical Immunology 110(4) (2002) 667-8.. [doi: 10.1067/mai.2002.128279](https://doi.org/10.1067/mai.2002.128279).
- [15] M. Smiri, A. Chaoui, N. Rouhier, E. Gelhaye, J-P. Jacquot and E. El Ferjani, Does Dithiothreitol affect cells and soluble mediators in the treatment of sputum, a modified methodology for treating sputum. Biological Trace Element Research 142(1) (2010) 93-105 . [DOI:10.1007/s12011-010-8749-3](https://doi.org/10.1007/s12011-010-8749-3)
- [16] National Research Council of Canada. Sulphur and its inorganic derivatives in the Canadian environment. NRC (1977) No. 15015
- [17] J.E. McKee and H.W. Wolf, Water quality criteria. Resources Agency of California State Water Resources Control Board. (1963). [https://www.waterboards.ca.gov/publications\\_forms/publications/general/docs/waterquality\\_criteria1963.pdf](https://www.waterboards.ca.gov/publications_forms/publications/general/docs/waterquality_criteria1963.pdf)
- [18] Y. Guesmi, R. Lafi, H. Agougui, M. Jabli, A. Oun, S. Majumdar and A. Hafiane, Synthesis and characterization of alpha alumina-natural apatite based porous ceramic support for filtration application. Materials Chemistry and Physics 122067 (2019). <https://doi.org/10.1016/j.molliq.2017.11.113>
- [19] A. Maurel, Techniques de l'ingénieur, osmose inverse, nanofiltration, ultrafiltration, tangential microfiltration-Considération théorique, in Techniques de l'ingénieur, (1993) 1-24. <https://www.techniques-ingenieur.fr/>
- [20] N. Zaghbani, Etude de la rétention des colorants par ultrafiltration assistée par les tensioactifs, PhD thesis, FST. (2010).
- [21] P. Aimer, P. Bacchin and A. Maurel, Filtration membranaire (OI, NF, UF, MFT) - Aspects théoriques: mécanismes de transfert, Technique de l'ingénieur. (2012). <https://www.techniques-ingenieur.fr>
- [22] M. Metaiche, Technologie membranaire, Université de Bouira. (2014).
- [23] M. Mahdi, Optimisation desalination systems by reverse osmosis: design, operating parameters and numerical simulation, PhD thesis, Ecole Nationale Polytechnique d'Alger (2006).

- [24] C. Larchet, DHDR of the University of Paris XII. 1994.
- [25] Y. Lanteri, Transport through nanofiltration membranes: characterization of electrical and dielectric properties. (2009).
- [26] L. Chareyre, Development of new non-oxide membranes for the separation of hydrogen at high temperature (2012).
- [27] L. Chaabane-Dammak, Etude des propriétés physico-chimiques et de la microstructure des membranes échangeuses d'ions, modifiés ou non modifiés, en présence d'un solvant mixte eau-méthanol et à différentes températures, Thèse de l'université Paris XII Val de marne (2007).
- [28] J-J. Bimbenet, Génie des procédés alimentaires, des bases aux applications, Paris, (2002).
- [29] L. Kaba, Elaboration of nanofiltration membrane on a carbon/zeolite composite support, Thesis, University Houari Boumediene-Alger. (2014).
- [30] F. Bosc, Synthesis and characterization of thin films and photocatalytic and mesostructured membranes based on TiO<sub>2</sub> anatase, PhD thesis, University of Montpellier II. (2004).
- [31] L. Djafer, Etude d'un système autonome pour le traitement des eaux usées par les techniques membranaires. Membrane with photocatalytic effect based on TiO<sub>2</sub>, PhD thesis, University Hassiba Benbouali, Chlef. (2011).
- [32] S. Balta, A. Sotto, P. Luis, L. Benea, B. Van Der Bruggen and J.J. Kim, A new outlook on membrane enhancement with nanoparticles: The alternative of ZnO. Membrane Science 389, (2012) 155–161.  
[https://www.cheric.org/research/tech/periodicals/doi.php?art\\_seq=1233372](https://www.cheric.org/research/tech/periodicals/doi.php?art_seq=1233372)
- [33] K.H. Tam, A.B. Djuriscic, C.M.N. Chan, Y. Xi, C.W. Tse, Y.H. Leung, W.K. Chan, F.C.C. Leung and D.W.T. Au, Antibacterial Activity of ZnO Nanorods Prepared by a Hydrothermal Method, Thin Solid Films 516 (2008) 6167.
- [34] N. Daneshvar, S. Aber, D.M.S. Seyed, A.R. Khataee and M.H. Rasoulifard,

- Photocatalytic degradation of the insecticide diazinon in the presence of prepared nanocrystalline ZnO powders under irradiation of UV-C light. *Journal of Chemical, Environmental and Biological Engineering* 1 (2008) 1-25.  
<http://www.znu.ac.ir/members/absjpaperEn/1515>
- [35] R. Yu, J. Wu, M. Liu, G. Zhu, L. Chen, Y. Chang and H. Lu, Toxicity of binary mixtures of metal oxide nanoparticles to *Nitrosomonas europaea*. *Chemosphere* 153 (2006) 187- 197.
- [36] L.H. Li, J.C. Deng, H.R. Deng, Z.L. Liu and L. Xin, Synthesis and characterization of chitosan/ZnO nanoparticle composite membranes. *Carbohydrate Research* 345 (2010) 994-998. DOI: [10.1016/j.carres.2010.03.019](https://doi.org/10.1016/j.carres.2010.03.019)
- [37] M.G. Nair, M. Nirmala, K. Rekha and A. Anukaliani, Fabrication of Polysulfone/ZnO Membrane: Influence ZnO Nanoparticles on Membrane Characteristics, *Materials Letters* 65 (2011) 1797. DOI: [10.1016/j.matlet.2011.03.079](https://doi.org/10.1016/j.matlet.2011.03.079)
- [38] K. Nakata and A. Fujishima, TiO<sub>2</sub> photocatalysis; Design and application, *Journal of Photochemistry and Photobiology C: Photochemistry Reviews* (2012) 169-189.  
<https://doi.org/10.1016/j.jphotochemrev.2012.06.001>
- [39] M. Tomino, K. Nagano, T. Hayashi, K. Kuroki and T. Kawai Antimicrobial efficacy of gutta percha supplemented with cetylpyridinium chloride, *Journal of Oral Science* 58 (2016) 277-282. DOI: [10.2334/josnusd.15-0620](https://doi.org/10.2334/josnusd.15-0620).
- [40] E.A. Abdel-aal, M.M. Rashad, A.N. El-Shazly, I.A. Ibrahim and M.F. El-Shahat, Hydrometallurgical treatment of non-sulfide zinc ore for precipitation of zinc oxide nanoparticles, *Physicochemical Problems of Mineral Processing* 52 (2016) 729-737.  
<http://www.minproc.pwr.wroc.pl/journal/pdf/ppmp52-2.729-737.pdf>
- [41] R. Wahab, F. Khan, Y.B. Yang, I.H. Hwang, H.S. Shin, J. Ahmad, S. Dwivedi, S.T. Khan, M.A. Siddiqui, Q. Saquib, J. Musarrat, A.A. Al-Khedhairy, Y.K. Mishrai and B.A. Alibj, Zinc oxide quantum dots: multifunctional candidates for arresting C2C12 cancer cells and their role towards caspase 3 and 7 genes, *RSC Advances* . 6 (2016) 26111- 26120.

- [42] B.D. Boruah and A. Misra, Conjugated assembly of colloidal zinc oxide quantum dots and multiwalled carbon nanotubes for an excellent photosensitive ultraviolet photodetector, *Nanotechnology* 27 (2016) 355204-355212.
- [43] T. Ktari, C. Larchet and B. Auclair, Etude du mécanisme de transfert de la dialyse ionique croisé. *European Polymer Journal* 34(10) (1998) 1415-1421.
- [44] D.B. Maouia, A. Boubakri, A. Hafane and S. Bouguecha, Aluminum Sulfate as an Innovative Draw Solute for Forward Osmosis Desalination. *Chem. Africa*. (2019).
- [45] H. Chemingui, S. Rezma, R. Lafi, Z. Alhalili, T. Missaoui, I. Harbi, M. Smiri, A. Hafiane, *International Journal of Environmental Analytical Chemistry* (2021). DOI: 10.1080/03067319.2021.1897121.
- [46] H. Chemingui, M. Smiri, T. Missaoui and A. Hafiane, Zinc Oxide Nanoparticles Induced Oxidative Stress and Changes in the Photosynthetic Apparatus in Fenugreek (*Trigonella foenum graecum* L.). *Bull. Environ. Contam. Toxicol.* 102, 477 (2019). doi:10.1007/s00128-019-02590-5.
- [47] J. Archana, M. Navaneethan, Y. Hayakawa, Morphological transformation of ZnO nanoparticle to nanorods via solid– solid interaction at high temperature annealing and functional properties. *Scr Mater* 113 (2016) 163–166.
- [48] H. Benhaddou, Separation and pre-concentration of Ni(II) and Co(II) by the Volumic Liquid Membrane (VLM) technique. Master thesis, université aboubekr belkaid, Tlemcen (2014).
- [49] M. Dellali, Elaboration and implementation of polymer membranes (PS, PMMA), activated carbon and their application in the treatment of lead and aluminium, Master thesis, Hassiba Benbouali-Chlef University. (2011).
- [50] M.E. Anderson, Determination of glutathione and glutathione disulfide in biological samples. *Methods in Enzymology* 113 (1985) 54855.
- [51] H. Chemingui, T. Missaoui, J. Mzali, T. Yildiz, M. Konyar, M. Smiri, N. Saiidi, A. Hafiane and H.C. Yatmaz, Facile green synthesis of Zinc oxide nanoparticles (ZnO NPs): Antibacterial and photocatalytic activities. *Materials Research Express* 6, 1050b4

- (2019). doi:10.1088/2053-1591/ab3cd6.
- [52] A. Moulahi, F. Sediri, Pencil-like zinc oxide micro/nano-scale structures: Hydrothermal synthesis, optical and photocatalytic properties. *Materials Research Bulletin*, 48(10) (2013) 3723–3728. doi:10.1016/j.materresbull.2013.05.116.
- [53] F. Liu, B. Yi, D. Xing, J. Yu, H. Zhang Nafion/PTFE composite membranes for fuel cell applications. *Journal of Membrane Science* 212(1–2) (2003) 213–223. [https://doi.org/10.1016/S0376-7388\(02\)00503-3](https://doi.org/10.1016/S0376-7388(02)00503-3)
- [54] R. Mahendran, R. Malaisamy, D.R. Mohan, Cellulose acetate and polyethersulfone blend ultrafiltration membranes. Part I: Preparation and characterizations. *Polymers for Advanced Technologies*, 15(3) (2004) 149–157. doi:10.1002/pat.417
- [55] M. Sivakumar, A.K. Mohanasundaram, D. Mohan, K. Balu, R. Rangarajan, Modification of cellulose acetate: Its characterization and application as an ultrafiltration membrane. *Journal of Applied Polymer Science*, 67(11), (1998) 1939–1946. doi:10.1002/(sici)1097-4628(19980314)67:11<1939: aid-app13>3.0.co;2-p
- [56] J.-H. Kim, K.-H. Lee, Effect of PEG additive on membrane formation by phase inversion. *Journal of Membrane Science*, 138(2), (1998) 153–163. doi:10.1016/s0376-7388(97)00224-x
- [57] L. Shen, X. Bian, X. Lu, L. Shi, Z. Liu, L. Chen, Z. Hou, K. Fan, Preparation and characterization of ZnO/ polyethersulfone (PES) hybrid membranes. *Desalination* 293 (2012) 21–29. doi:10.1016/j.desal.2012.02.019
- [58] S. Balta, A. Sotito, P. Luis, L. Benea, B. Van der Bruggen, J. Kim, A new outlook on membrane enhancement with nanoparticles: The alternative of ZnO. *Journal of Membrane Science* 389 (2012) 155–161.
- [59] S., Wongsasulak, M., Patapeejumruswong, J., Weiss, P., Supaphol, T. Yoovidhya, Electrospinning of food-grade nanofibers from cellulose acetate and egg albumen blends. *Journal of Food Engineering* 98(3) (2010) 370–376. doi:10.1016/j.jfoodeng.2010.01.014
- [60] X., Sui, C., Shao, Y. Liu, Photoluminescence of polyethylene oxide–ZnO composite electrospun fibers. *Polymer*, 48(6) (2007) 1459–1463. doi:10.1016/j.polymer.2007.01.039

- [61] M.N. Abu Semana, M. Khayet and N. Hilal, Nanofiltration thinfilm composite polyester polyether sulfone-based membranes prepared by interfacial polymerization. *Journal of Membrane Science* 348 (2010) 109. DOI: [10.1080/19443994.2013.774113](https://doi.org/10.1080/19443994.2013.774113)
- [62] R.J. Mansouri and V. Chen, The effects of mechanical and chemical modification of TiO<sub>2</sub> nanoparticles on the surface chemistry, structure and fouling performance of PES ultrafiltration membranes *Journal of Membrane Science* 378(1-2) (2011) 73.
- [63] H.Y. Choi, J.H. Bae, Y. Hasegawa, S. An, I.S. Kim, H. Lee, M. Kim, Thiol-Functionalized Cellulose Nanofiber Membranes for the Effective Adsorption of Heavy Metal Ions in Water. *Carbohydrate Polymers*, 115881(2020). doi:10.1016/j.carbpol.2020.115881
- [64] Safety Data Sheet of the International Program on Chemical Safety, Titanium Dioxide, 2009.
- [65] Scientific Committee on Consumer Safety (SCCS), Opinion on ZnO, 2012.
- [66] M. Šimundić, B. Drašler, V. Šuštar, J. Zupanc, R. Štukelj, et al. Effect of engineered TiO<sub>2</sub> and ZnO nanoparticles on erythrocytes, platelet-rich plasma and giant unilamellar phospholipid vesicles. *BMC Veterinary Research* 9 (2013) 7. DOI: [10.1186/1746-6148-9-7](https://doi.org/10.1186/1746-6148-9-7).
- [67] E. Heikkilä, H. Martinez-Seara, A.A. Gurtovenko, I. Vattulainen and J. Akola, Atomistic simulations of anionic Au 144 (SR) 60 nanoparticles interacting with asymmetric model lipid membranes. *Biochimica et Biophysica Acta* 1838(11) (2014) 2852-2860. DOI: [10.1016/j.bbamem.2014.07.027](https://doi.org/10.1016/j.bbamem.2014.07.027)
- [68] N. Grinceviciute, D. Verdes and V. Snitka, Effect of Zinc Oxide and Titanium Dioxide Nanoparticles on Supported Lipid Bilayers, *Journal of Nanomedicine Research* 2(3) (2015) 30. <http://medcraveonline.com/JNMR/JNMR-02-00030.pdf>

**Table 1.** The composition of casting solutions.

Membrane	DMF(g)	CA (g)	PEG-1000 (g)	Nanoparticles (g)
M <sub>0</sub>	20	4	1	0
M <sub>1</sub> ( CA/ZnO NPs)	20	4	1	0.1
M <sub>2</sub> ( CA/TiO <sub>2</sub> NPs)	20	4	1	0.1

**Table 2.** Measurement of permeability fluxes of AC, AC-ZnO and AC-TiO<sub>2</sub> membranes.

<b>AC membrane</b>				
P (bar)	2	3	4	5
S (m <sup>2</sup> )	0.0028	0.0028	0.0028	0.0028
V (L)	0.0030	0.0030	0.0030	0.0030
Time (h)	0.0811	0.0475	0.0349	0.0217
J (L/m <sup>2</sup> /h)	13.089	22.348	30.417	48.920
<b>AC-TiO<sub>2</sub> membrane</b>				
P (bar)	2	3	4	5
S (m <sup>2</sup> )	0.0028	0.0028	0.0028	0.0028
V (L)	0.0030	0.0030	0.0030	0.0030
Time (h)	0.0852	0.0577	0.0450	0.0349
J (L/m <sup>2</sup> /h)	12.459	18.398	23.590	30.417
<b>AC-ZnO membrane</b>				
P (bar)	2	3	4	5
S (m <sup>2</sup> )	0.0028	0.0028	0.0028	0.0028
V (L)	0.0030	0.0030	0.0030	0.0030
Time (h)	0.0097	0.0075	0.0061	0.0038
J (L/m <sup>2</sup> /h)	109.21	141.54	173.74	272.89

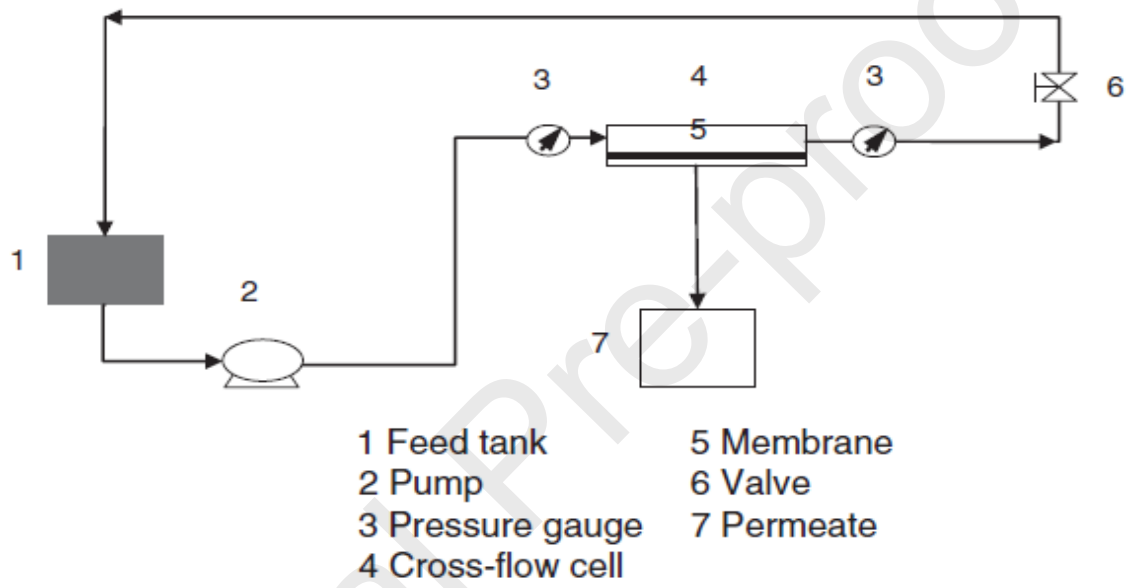


**Figure 1.** Scheme of the experimental system

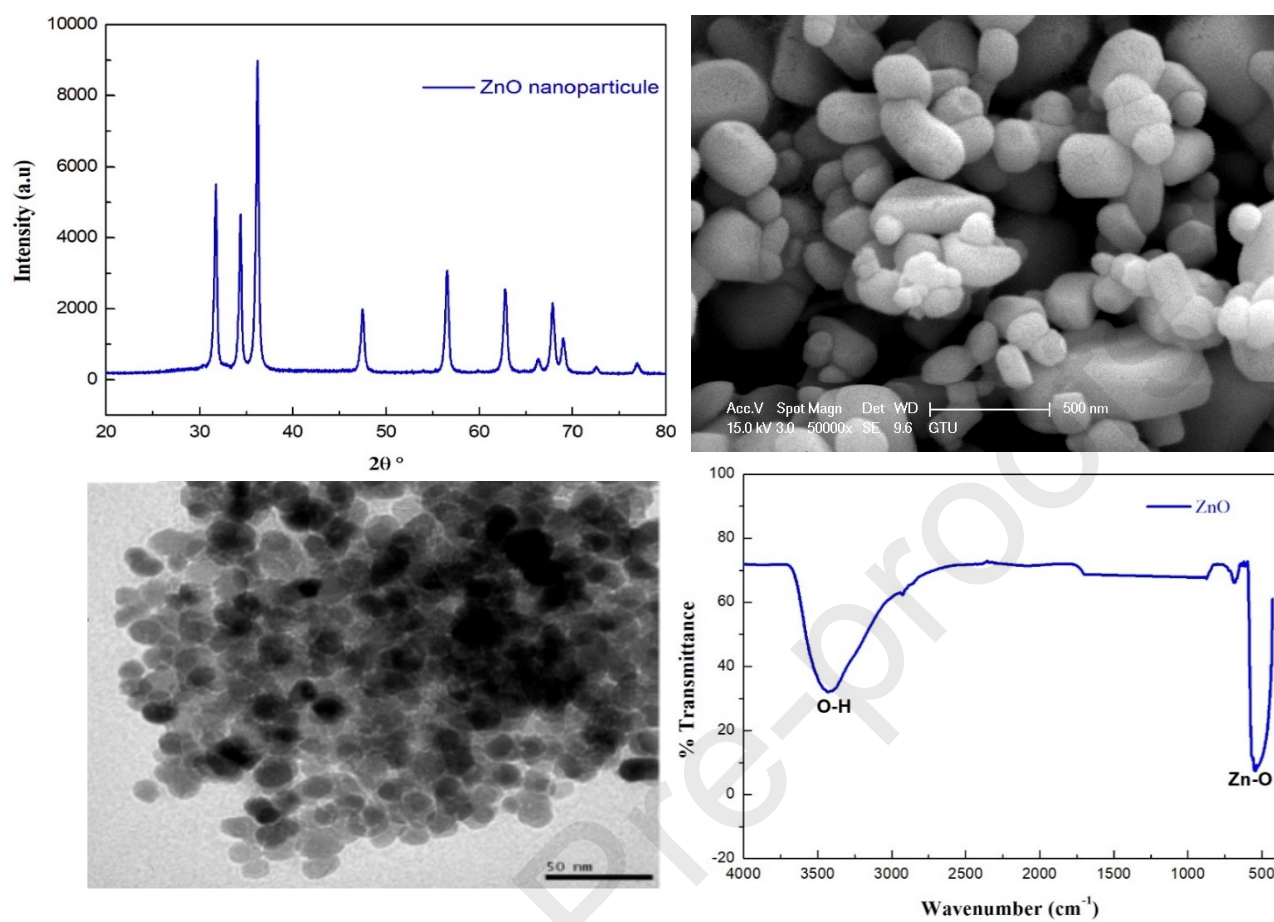


**Figure 2.** XRD patterns (a), SEM (b), TEM (c), and FTIR (d) of Zinc oxide nanoparticle

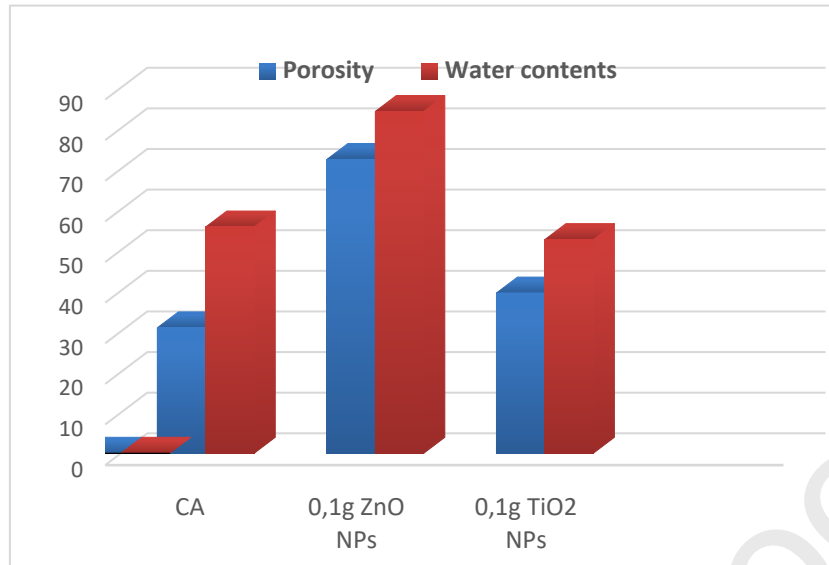


**Figure 3.** Porosity and water content of the bare CA and the blended NPs CA.

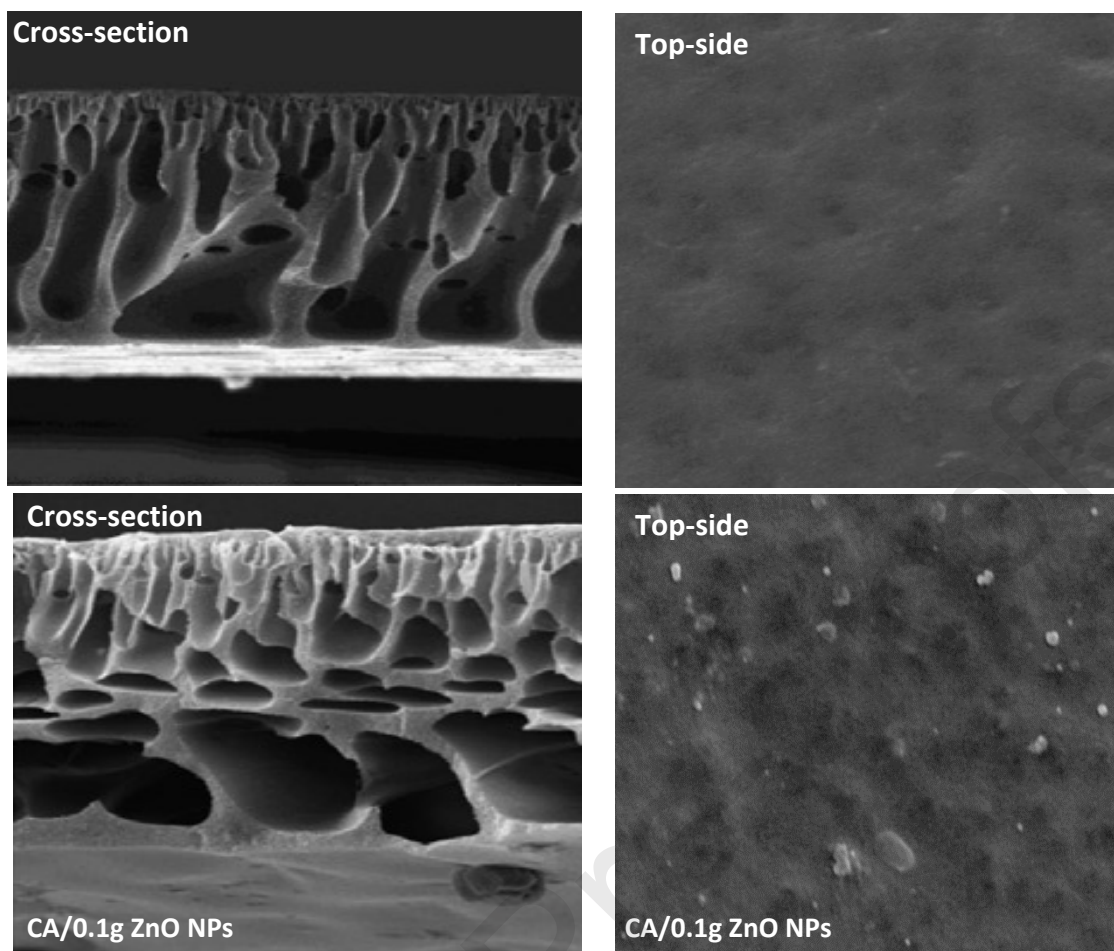


**Figure 4.** SEM images of the bare Cellulose acetate and the ZnO blended CA Membranes.

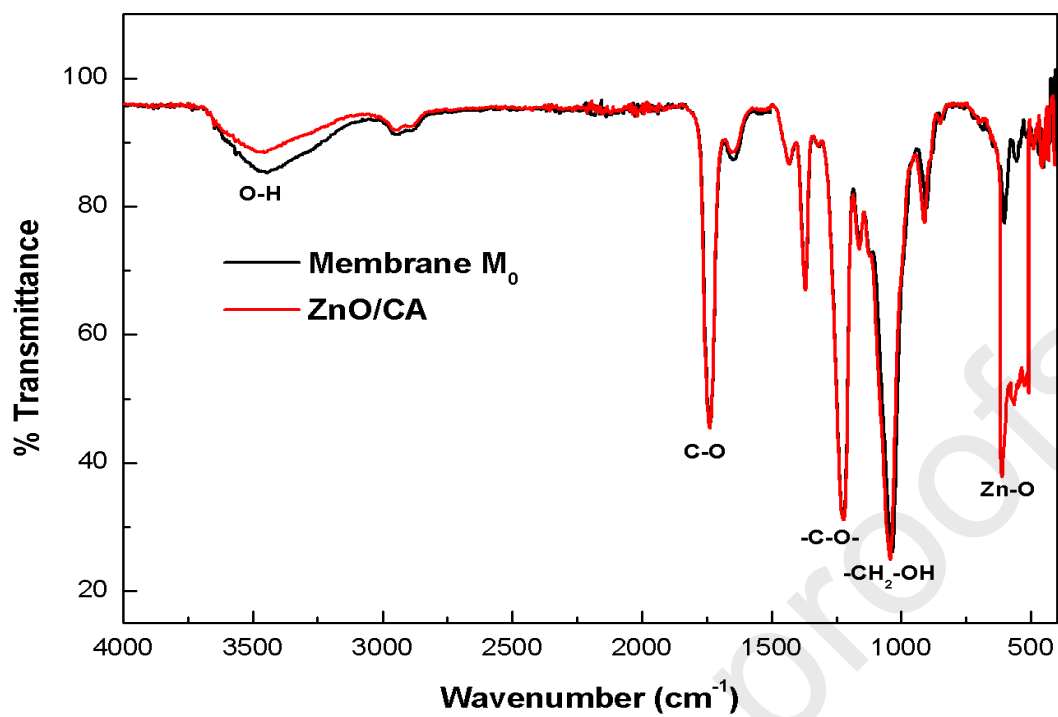


**Figure 5.** FTIR spectrum (a) Pure Membrane M<sub>0</sub> (b) ZnO/CA membrane.

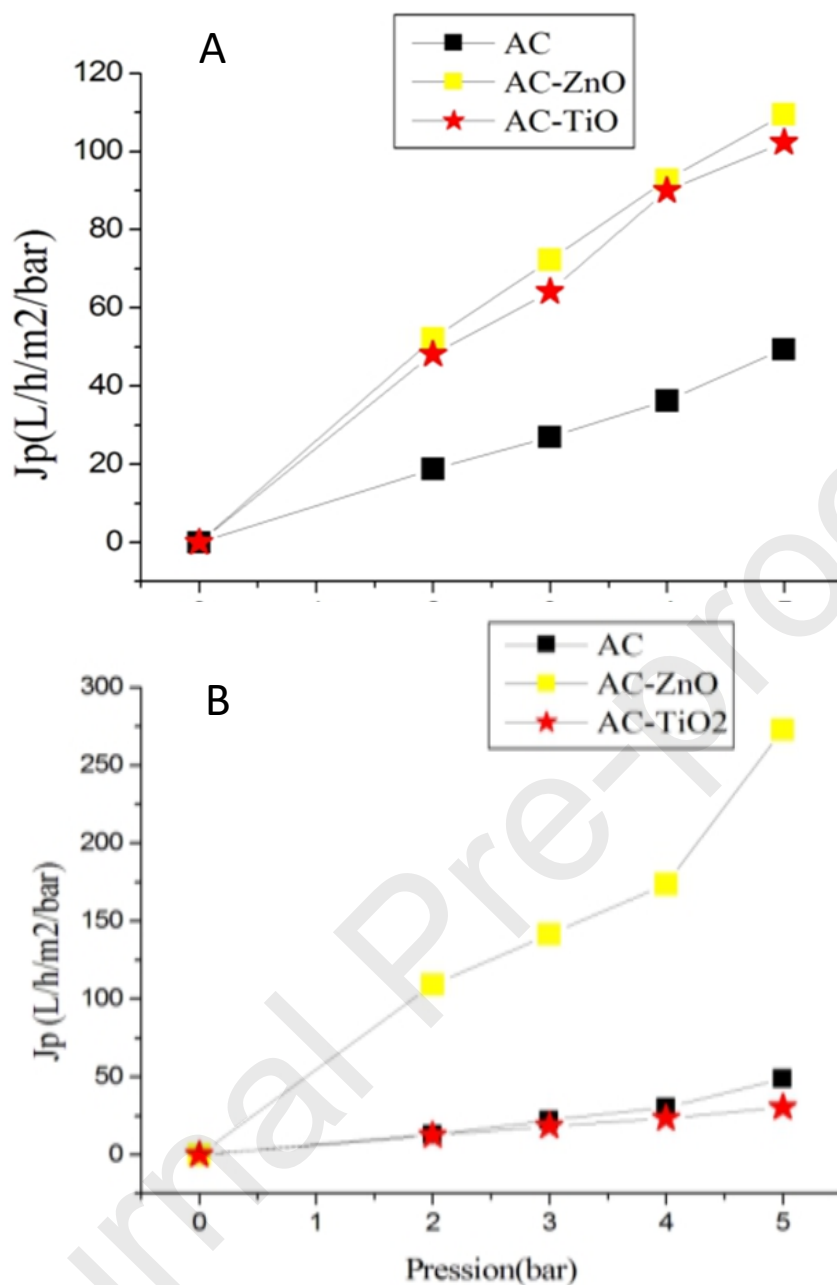


**Figure 6.** Effect of transmembrane pressure on (A) water and (B) DTT flow of AC, AC-ZnO, and AC-TiO<sub>2</sub> membranes.

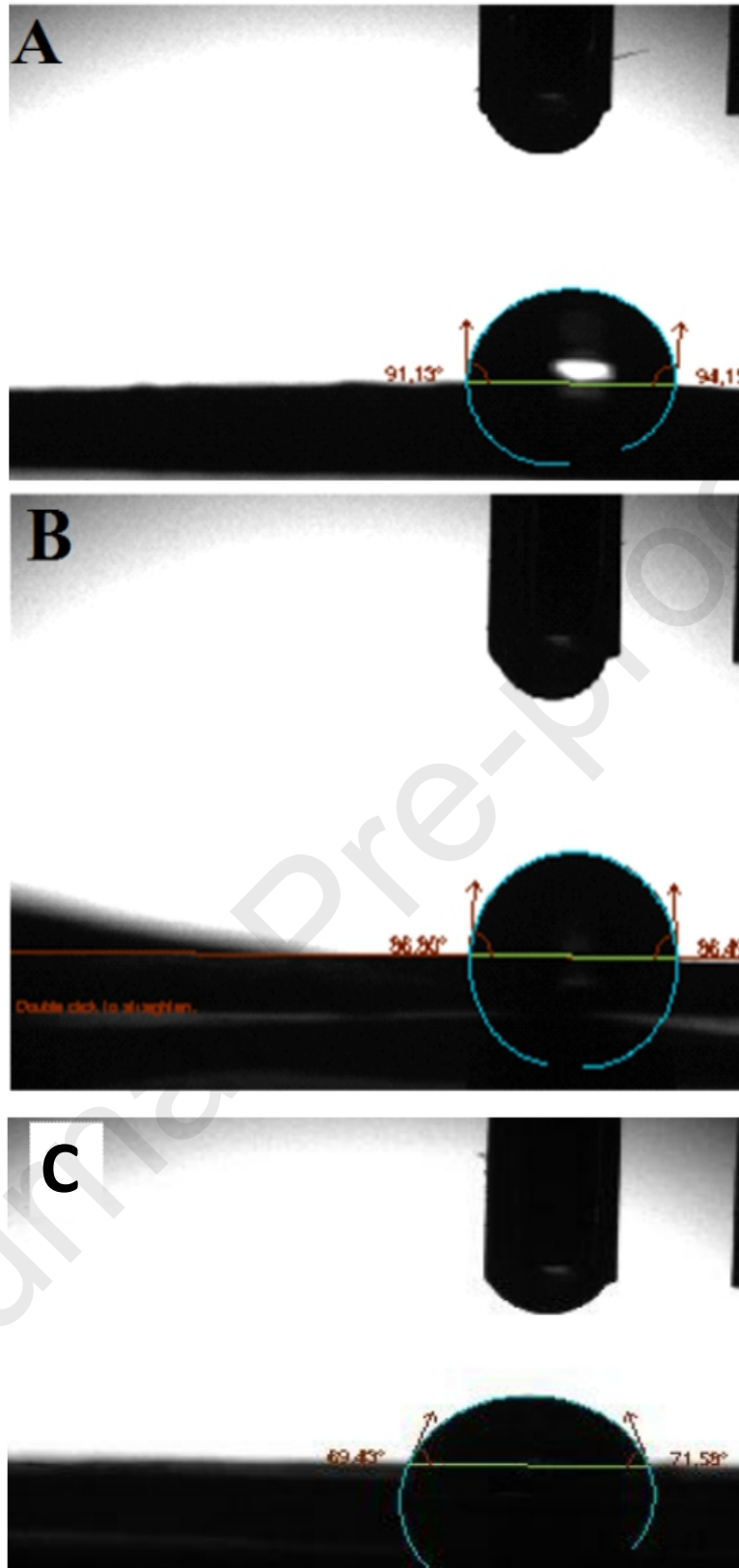


**Figure 7.** Profile of water drops on membrane surfaces: (A) AC, (B) AC-TiO<sub>2</sub>, and (C) AC-ZnO membranes.

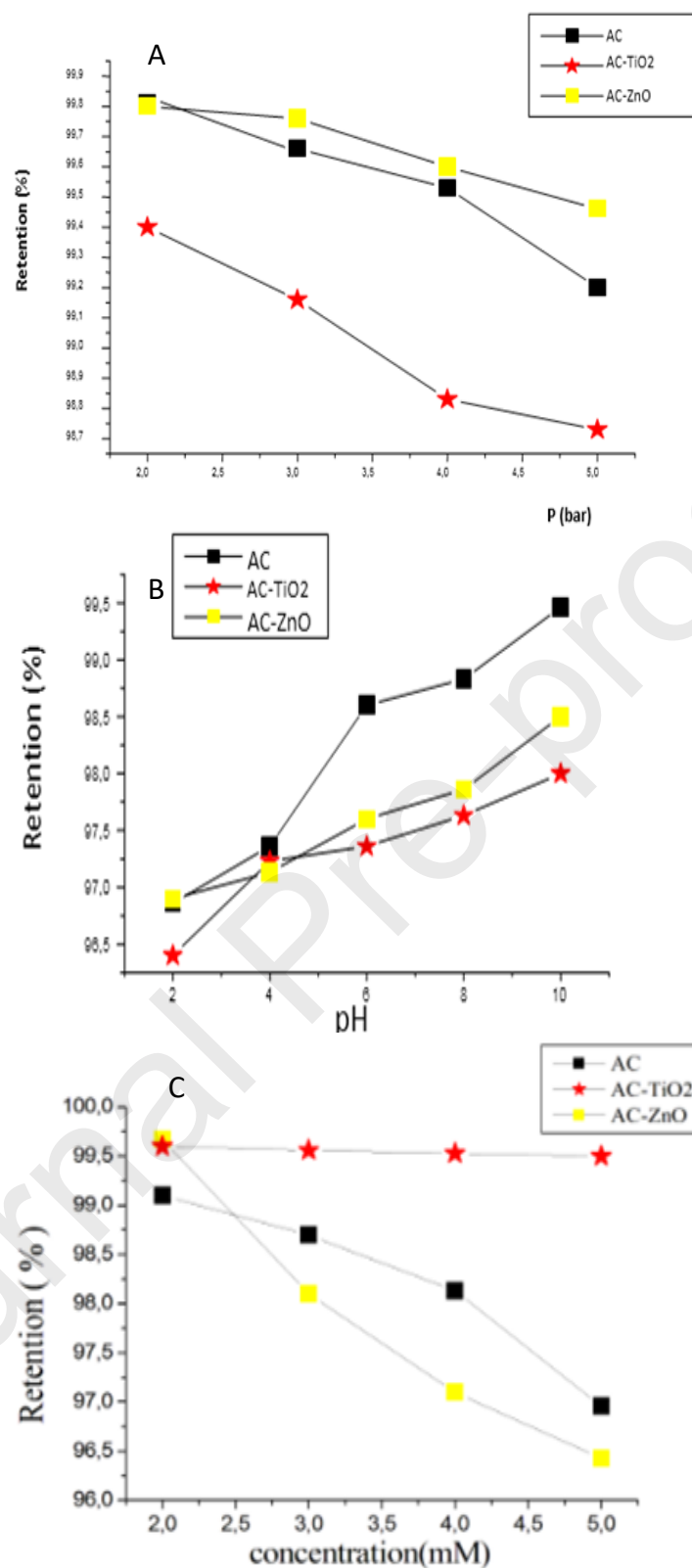


**Figure 8.** Effect of (A) transmembrane pressure, (B) pH, and (C) DTT concentration on permeate retention of thiol by ultrafiltration assisted ZnO and TiO<sub>2</sub> NPs membranes.

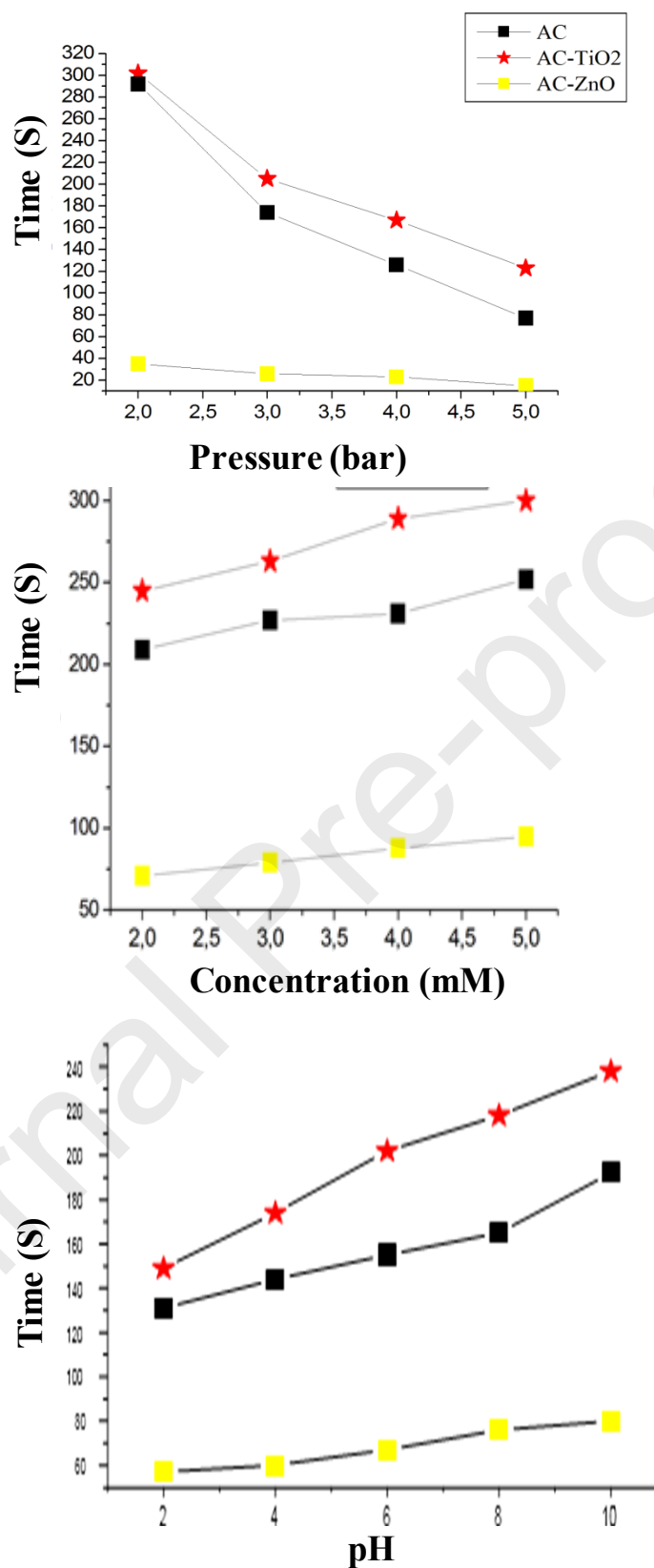


**Figure 9.** Effect of time on thiol retention by ultrafiltration membrane assisted ZnO and TiO<sub>2</sub> NPs under different pressures, DTT concentrations, and pH.

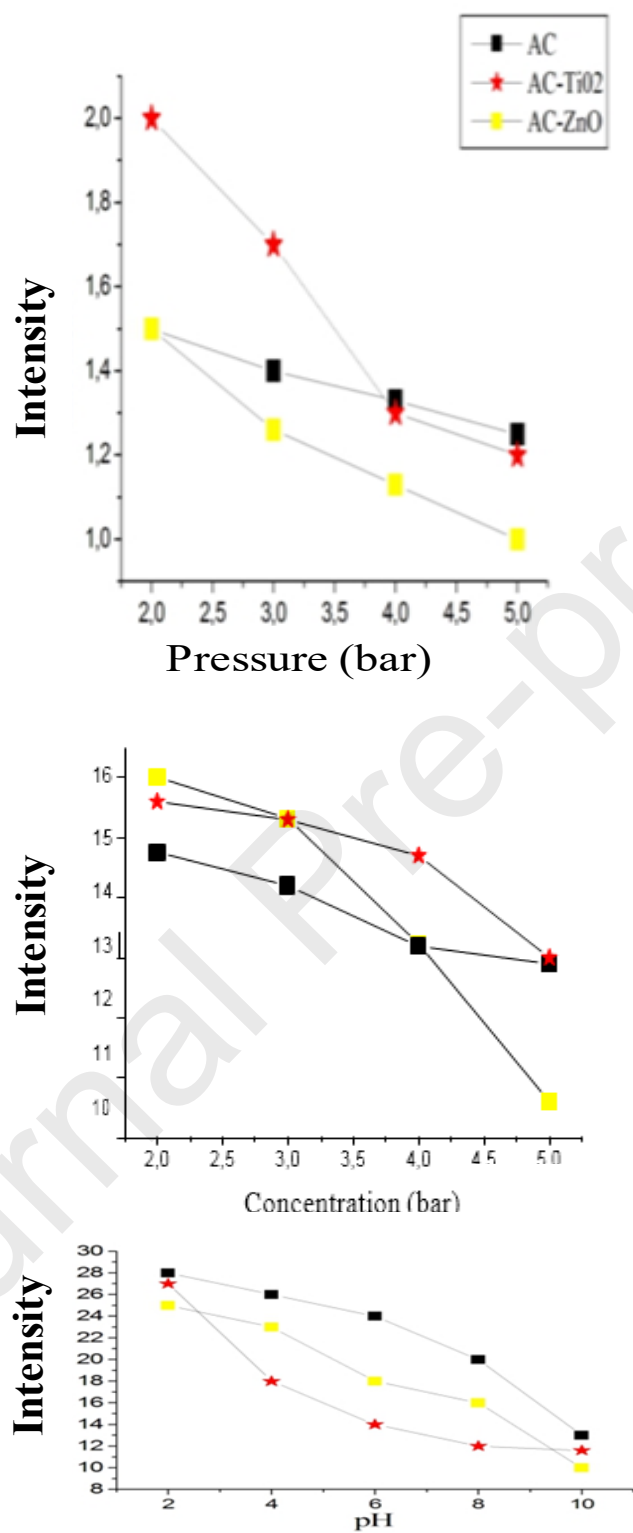


**Figure 10.** The intensity of thiols identified by fluorescence spectrum in permeate obtained by ultrafiltration membrane assisted ZnO and TiO<sub>2</sub> NPs.

## **CONFLICTS OF INTEREST**

The authors declare they have no conflict of interest.

Journal Pre-proofs